


RESEARCH ARTICLE

Intrinsic connectivity networks underlying individual differences in control-averse behavior

Sarah Rudolf^{1,2}  | Thomas Baumgartner^{1,2} | Sebastian Markett³ | Katrin Schmelz^{4,5} | Roland Wiest⁶ | Urs Fischbacher^{4,5} | Daria Knoch^{1,2}

¹Department of Social Psychology and Social Neuroscience, Institute of Psychology, University of Bern, Bern, Switzerland

²Center for Cognition, Learning and Memory, University of Bern, Bern, Switzerland

³Molecular Psychology, Department of Psychology, Humboldt University Berlin, Berlin, Germany

⁴Department of Economics, University of Konstanz, Konstanz, Germany

⁵Thurgau Institute of Economics, Kreuzlingen, Switzerland

⁶Department of Neuroradiology, Inselspital, Bern, Switzerland

Correspondence

Sarah Rudolf, Department of Social Psychology and Social Neuroscience, Institute of Psychology, University of Bern, Fabrikstrasse 8, 3012 Bern, Switzerland.
Email: sarah.rudolf@psy.unibe.ch

Funding information

Mens Sana Foundation

Abstract

When people sense that another person tries to control their decisions, some people will act against the control, whereas others will not. This individual tendency to control-averse behavior can have far-reaching consequences, such as engagement in illegal activities or noncompliance with medical treatments. Although individual differences in control-averse behavior have been well documented in behavioral studies, their neurological basis is less well understood. Here, we use a neural trait approach to examine whether individual differences in control-averse behavior might be linked to stable brain-based characteristics. To do so, we analyze the association between intrinsic connectivity networks as measured by resting state functional magnetic resonance imaging and control-averse behavior in an economic exchange game. In this game, subjects make choices that are either free or controlled by another person, with real consequences to both interaction partners. We find that the individual level of control-averse behavior can be positively predicted by intrinsic connectivity within the salience network, but not the central executive network or the default mode network. Specifically, subjects with a more prominent connectivity hub in the dorsal anterior cingulate cortex show greater levels of control-averse behavior. This finding provides the first evidence that the heterogeneity in control-averse behavior might originate in systematic differences of the stable functional brain organization.

KEYWORDS

control aversion, intrinsic connectivity networks, resting state fMRI, neural trait, salience network, anterior cingulate cortex

1 | INTRODUCTION

Control-averse behavior is a highly relevant social phenomenon, contributing to prevalent detrimental behaviors such as tax evasion (Mendoza, Wielhouwer, & Kirchler, 2017; Murphy, 2005) or noncompliance with vaccination recommendations (Betsch & Böhm, 2016). It describes the tendency to react negatively to exogenous control of one's freedom of choice (Falk & Kosfeld, 2006). In other words, when people sense that another person tries to control their decisions, some people will act against the control, whereas others will not. Moreover, control-averse behavior can have far-reaching consequences for the individual, such as noncompliance with psychiatric treatments (De las Cuevas, Peñate, Betancort, & de Rivera, 2014) or engagement in illegal or harmful activities (Hornik, Jacobsohn, Orwin, Piesse, &

Kalton, 2008; Wiium, Aarø, & Hetland, 2009). Importantly, individuals differ in the extent of their control-averse behavior (Falk & Kosfeld, 2006; Ziegelmeyer, Schmelz, & Ploner, 2012), but the origin of this heterogeneity is less well understood. Whereas previous work has associated control aversion with negative affects and a sense of being restricted in one's freedom of choice (Dillard & Shen, 2005; Miron & Brehm, 2006), more recent work has highlighted the role of social cognitions, such as perceived distrust, in driving control-averse behavior in social interactions (Falk & Kosfeld, 2006; Rudolf et al., 2018). To date, however, little is known about the underlying neurobiological basis of individual differences in control-averse behavior.

One way to quantify the neurobiology of individual differences in control-averse behavior is to study stable brain-based characteristics, termed neural traits (Nash, Gianotti, & Knoch, 2015). A fruitful

approach to investigating neural traits has been the characterization of functionally interconnected brain networks at rest, so-called intrinsic connectivity networks (ICNs) (Biswal, Yetkin, Haughton, & Hyde, 1995; Markett, Montag, & Reuter, 2018; Seeley et al., 2007; Xiong, Parsons, Gao, & Fox, 1999). ICNs are networks of remote brain regions that show a strong coupling of spontaneous fluctuations in the blood oxygen level-dependent (BOLD) signal typically measured with resting state functional magnetic resonance imaging (fMRI) (Gordon, Stollstorff, & Vaidya, 2012; Menon, 2011; Seeley et al., 2007; Van den Heuvel & Hulshoff Pol, 2010). The major ICNs at rest correspond closely to functional networks during active tasks (Smith et al., 2009), implying that ICNs relate to “online” functioning that underlies central aspects of human behavior. Furthermore, the temporal and spatial signatures of ICNs have been shown to predict individual differences in behavior (Fox, Snyder, Vincent, & Raichle, 2007; Kelly, Uddin, Biswal, Castellanos, & Milham, 2008; Mennes et al., 2011; Seeley et al., 2007). Importantly, ICNs are remarkably stable across time and samples (Biswal et al., 2010; Damoiseaux et al., 2006; Shehzad et al., 2009; Zuo et al., 2010) and can be used to distinguish between individual profiles (Finn et al., 2015; Tavor et al., 2016). They therefore meet the criteria of stable brain-based characteristics that may help explain the neurobiological basis of the heterogeneity in social behavior, as formalized in the neural trait approach (Nash et al., 2015).

Three ICNs are particularly relevant for the cognitive and emotional information processing underlying social behavior: the central executive network (CEN), the salience network (SN), and the default mode network (DMN) (Menon, 2011). The CEN, also referred to as the frontoparietal network (Smith et al., 2009), consists primarily of nodes in the dorsolateral prefrontal cortex (dlPFC) and the lateral posterior parietal cortex (PPC) and has been associated with high-level cognitive functions such as planning, goal-directed decision making, and working memory (Menon, 2011; Seeley et al., 2007; White, Joseph, Francis, & Liddle, 2010; Yu et al., 2017). The SN, also referred to as the cingulo-opercular network (Chen et al., 2013; Elton & Gao, 2014; Hahn et al., 2015) or the executive control network (Smith et al., 2009), is anchored in the dorsal anterior cingulate cortex (ACC) and the anterior insula and has been associated with the detection of and orientation to salient external stimuli as well as the autonomic integration of internal events (Menon, 2011; Seeley et al., 2007). Moreover, recent findings suggest that the SN may be responsible for switching between the engagement of the CEN and the DMN during events that require access to attention and working memory resources (Menon & Uddin, 2010; Sridharan, Levitin, & Menon, 2008). Lastly, the DMN has its most prominent nodes in the medial prefrontal cortex (mPFC), the posterior cingulate cortex (PCC) and the medial temporal lobes (Andrews-Hanna, Reidler, Sepulcre, Poulin, & Buckner, 2010; Greicius, Krasnow, Reiss, & Menon, 2003; Menon, 2011; Raichle et al., 2001) and has been associated with self-related cognitive activity, such as self-monitoring, and social cognition (Li, Mai, & Liu, 2014; Mars et al., 2012; Menon, 2011). Although the DMN is the ICN that is predominantly associated with social cognitive functions, recent work has highlighted the roles of the SN and CEN in predicting reciprocal social behavior (Cáceda, James, Gutman, & Kilts, 2015) and tendencies for cooperative behavior (Hahn et al., 2015). Similarly,

control-averse behavior in social interactions relies on social cognitive functions and choosing between cooperative and noncompliant social behavior (Falk & Kosfeld, 2006; Rudorf et al., 2018). Taken together, their contribution to these central aspects of human social behavior makes the CEN, SN, and DMN prime candidates for neural traits of control-averse behavior.

Here, we investigate the neural traits of control-averse behavior by combining a behavioral Control aversion task with independent resting state fMRI. In the Control aversion task, subjects make decisions that are either free or controlled by another person. In the Free condition, subjects can choose freely among a set of monetary allocations between themselves and the other person, ranging from selfish to more generous and fairer allocations. In the Controlled condition, the other person requests a minimal monetary return and thereby restricts the subjects' freedom of choice to the more generous and fairer allocations. The degree to which subjects allocate less money to the other person in the Controlled than in the Free condition measures their control-averse behavior. Crucially, the decisions are not hypothetical, but have real (monetary) consequences to both the subject as well as the other person. This feature ensures a high ecological validity of the measured control-averse behavior.

To assess the neural traits, we identify the CEN, SN, and DMN in resting state fMRI data using an independent component analysis (ICA). This approach has two advantages. First, ICNs measured by resting state fMRI instead of task-related fMRI are more robust to physiological noise and represent a reliable measurement of large-scale brain networks (Bressler & Menon, 2010; Menon, 2011). Second, in contrast to a seed-based analysis of connectivity with individual brain regions, the ICA allows us to investigate the dynamics of intrinsic brain networks at a larger scale (Van den Heuvel & Hulshoff Pol, 2010). By applying the ICA to the resting state fMRI data, we separate the BOLD signal into 70 statistically independent components with unique, albeit not exclusive, spatial, and temporal patterns (Abou Elseoud et al., 2011; Laird et al., 2017; Menon, 2011; Ray et al., 2013). Using a template matching procedure we then identify the CEN, SN, and DMN among the independent components (Shirer, Ryali, Rykhlevskaia, Menon, & Greicius, 2012; Smith et al., 2009). We focus on the CEN, SN, and DMN due to their implications in social cognitive functions and social behavior (Cáceda et al., 2015; Hahn et al., 2015; Mars et al., 2012), which make them likely candidates for neural traits of control-averse behavior in social interactions. The components that match visual, auditory and sensorimotor networks are omitted from the analysis, because we have no prior assumptions about their involvement in control-averse behavior. Finally, we test whether the spatial and temporal dynamics within and between the CEN, SN, and DMN can predict individual differences in control-averse behavior.

2 | MATERIALS AND METHODS

2.1 | Participants

We recruited a total of 61 students from the University of Bern for participation in this study. All participants were right-handed,

nonsmokers, and reported no history of psychological disorders, neurological, or cardiovascular diseases. We excluded students of psychology, economics and social sciences from participation to reduce the likelihood of prior knowledge of the concept of control aversion. Data from 11 participants had to be excluded from the analysis due to excessive movements during the resting state fMRI scan (movement >1.5 mm, or rotation $>1.5^\circ$). Data from the remaining 50 participants (28 female; mean, 22 ± 4 SD years) were included in the analysis. All participants received a compensation of CHF 50 (\approx USD 50) for participation in the study in addition to the payoff from the task described below. The study was approved by the Bern Cantonal Ethics Commission and all participants gave informed, written consent.

2.2 | Control aversion task and behavioral data analysis

To measure each individual's level of control-averse behavior, we implemented a Control aversion task based on a principal-agent game previously used in behavioral economics (Falk & Kosfeld, 2006; Schmelz & Ziegelmeyer, 2015; Ziegelmeyer et al., 2012). Subjects completed the task while they were lying in an MRI scanner as part of an omnibus project; the task-based fMRI data are reported elsewhere (Rudorf et al., 2018). In the Control aversion task, subjects are repeatedly asked to allocate money between themselves and an anonymous other person, called player A. Before a subject can make a decision, however, the player A chooses to either let the subject decide freely (Free condition) or to request a minimum monetary return from the subject and thereby restrict the subject's choice options (Controlled condition). The monetary allocations are presented as a set of five predefined pairs of monetary units (MUs), called generosity levels, ranging from a selfish allocation (99 MUs for the subject, 1 MU for player A) to a more generous and equal allocation (80 MUs for both the subject and player A) (Figure 1). In the Free condition, the subject

has the choice between all five generosity levels. In the Controlled condition, the subject's choice is restricted to levels two to five, meaning that the most selfish option is ruled out. The monetary allocations are designed such that choosing a higher generosity level is associated with higher profits for player A, making it beneficial for player A, and relatively small costs for the subject. Concretely, with increasing generosity levels, the MUs for player A increase in larger increments from 1 to 80 MUs, whereas the MUs for the subject decrease in smaller increments from 99 to 80 MUs. Moreover, the highest level represents an equal allocation and the largest sum of MUs. These features were implemented to motivate subjects to choose a high level when they can decide freely and, hence, to create room for the choice of a lower level in the Controlled condition. The contrast between the two conditions has been shown to evoke control-averse behavior: a substantial share of subjects will allocate less money to the other person if the other person restricts the subject's choices than when the subject can decide freely (Falk & Kosfeld, 2006; Schmelz & Ziegelmeyer, 2015; Ziegelmeyer et al., 2012). With regard to the Control aversion task, we define control-averse behavior as the difference between the chosen levels in the Free condition and the chosen levels in the Controlled condition. Subjects' choices were highly consistent within each condition, with a variance of mean 0.33 ± 0.33 SD, median 0.27, in the Controlled condition and a variance of mean 0.33 ± 0.38 SD, median 0.21, in the Free condition (Supporting Information Materials S3). Therefore, choices within each condition were aggregated and the individual level of control-averse behavior was computed as the difference between each subject's mean chosen level in the Free condition minus the mean chosen level in the Controlled condition. Thus, greater positive values correspond to a higher level of control-averse behavior. Critically, subjects differ in whether and to which degree they display control-averse behavior. Whereas some subjects will always choose the lowest possible level, others will choose the same

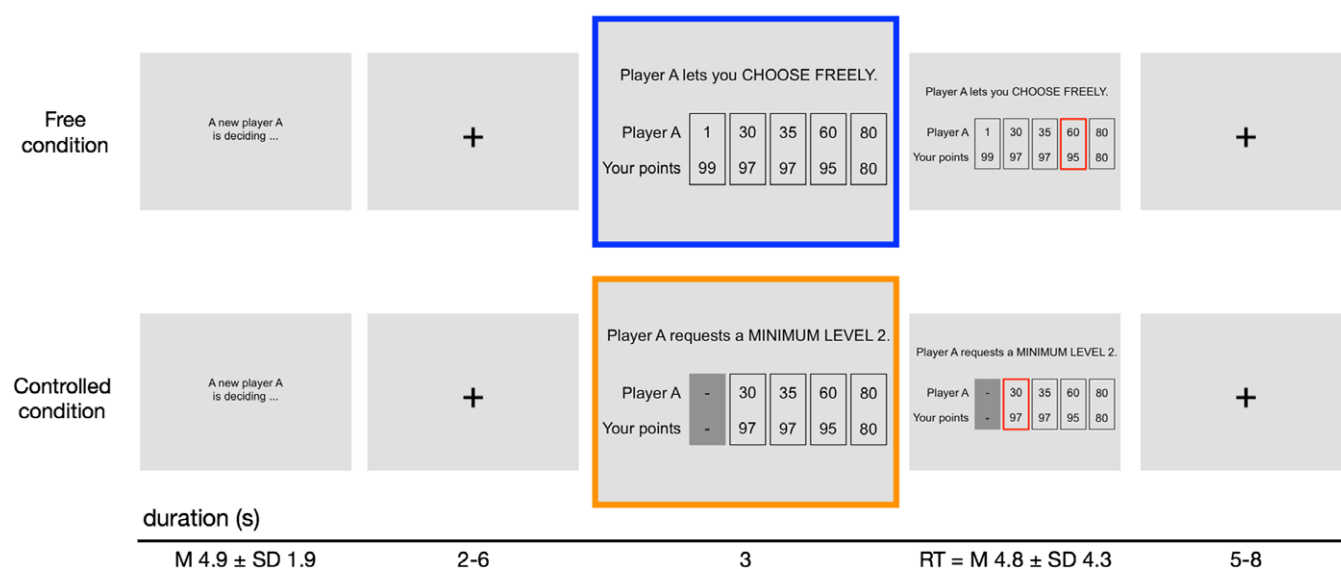


FIGURE 1 Control aversion task. At the beginning of each of 16 trials, the subject is reminded that a new player A is assigned. In the Free condition, the subject can choose freely among five levels of monetary allocations between herself and player A. In the Controlled condition, the player A requests a minimum of level two. After a delay of 3 s, a red selection frame appears around a random level and the subject selects a level by moving the frame and pressing an OK button. Interstimulus intervals were randomly jittered. RT, response time [Color figure can be viewed at wileyonlinelibrary.com]

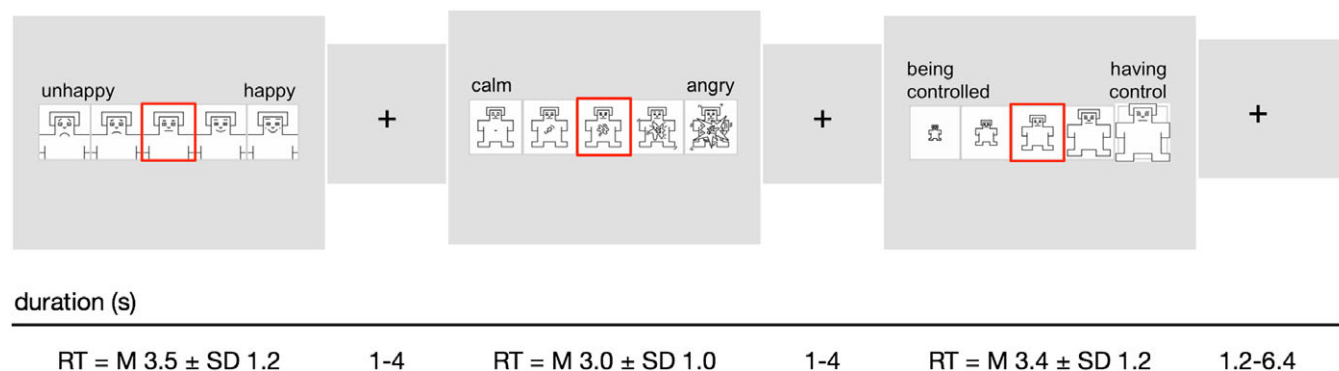


FIGURE 2 Trial-by-trial affect ratings. At the end of each trial, subjects rated their unhappiness, anger and feeling of being controlled on 5-point pictorial assessment scales (Bradley & Lang, 1994). The interstimulus intervals were randomly jittered. RT, response time [Color figure can be viewed at wileyonlinelibrary.com]

level in both conditions, and yet others will choose a lower level when they are controlled than when they can decide freely.

At the end of each trial, subjects are asked to rate their unhappiness, anger and feeling of being controlled on 5-point pictorial assessment scales (Figure 2) (Bradley & Lang, 1994). The feeling of being controlled scale was used as a manipulation check.

In total, subjects were presented with 16 anonymous players A's decisions from a pilot study, which were preselected to ensure an equal number of trials in the Free and in the Controlled condition, that is, eight trials per condition. Subjects were not aware of this preselection, but they were informed that the players A's decisions had been prerecorded for logistic reasons. Subjects were also informed that their choices in the task had real consequences in the sense that one trial would be randomly selected and paid out to themselves and the corresponding player A. Prior to performing the task, subjects read the instructions and were quizzed to ensure they had understood the task and its payoff scheme.

At the end of the task, one trial was randomly selected and the corresponding payoffs were converted into CHF (with 1 MU = CHF 0.20 \approx USD 0.20). Based on the task, the subjects' received a mean CHF 17.50 \pm 3.90 SD, and the players A received a mean CHF 10.70 \pm 4.60 SD.

The behavioral data were analyzed using the Statistics and Machine Learning Toolbox in MATLAB R2015b (The MathWorks, Inc.). Because the behavioral data did not follow normal distributions as assessed by Kolmogorov–Smirnov tests, paired samples were compared using Wilcoxon signed rank tests and correlations were assessed using Spearman's rho as well as robust regressions. For all robust regressions, the residuals were approximately normally distributed.

2.3 | MRI data acquisition

All MRI data were acquired on a Siemens Trio 3.0 Tesla whole-body scanner (Siemens, Erlangen) using a 32-channel head coil. The functional session started off with a localizer scan followed by a resting state fMRI sequence, during which subjects were instructed to lie as still as possible with their eyes closed, thinking of nothing in particular and without falling asleep. From each subject, we acquired gradient echo T2*-weighted echo-planar images (EPIs; 460 volumes per session)

with BOLD contrast (32 slices per volume, interleaved order, Field of View 192 \times 192 \times 108 mm, slice thickness 3 mm, gap 0.75 mm, repetition time 1,980 ms, echo time 30 ms, flip angle 90°). Volumes were acquired in axial orientation to the anterior commissure-posterior commissure line. After the functional run, high-resolution T1-weighted 3D modified driven equilibrium Fourier transformation (MDEFT) images were acquired from each subject (176 slices, Field of View 256 \times 256 \times 176 mm, slice thickness 1 mm, no gap, repetition time 7.92 ms, echo time 2.48 ms, flip angle 16°).

2.4 | Preprocessing

Preprocessing was implemented in the FMRIB Software Library (FSL) version 5.0.10 (Jenkinson, Beckmann, Behrens, Woolrich, & Smith, 2012) and ICA-AROMA (Pruim et al., 2015). Prior to preprocessing, all images were skull-stripped using the brain extraction tool (BET) included in FSL (Smith, 2002). The functional images were skull-stripped using BET with the extension for four-dimensional images and a fractional intensity of 0.3. For the anatomical images, we first removed the neck information using the FSL function robustfov and then skull-stripped the images using BET with a fractional intensity of 0.3. All images were visually inspected to ensure optimal results.

Preprocessing of the functional images involved the following steps: (1) removal of the first 10 volumes, (2) motion correction using FMRIB's Linear Image Registration Tool (MCFLIRT) (Jenkinson, Bannister, Brady, & Smith, 2002), (3) correction for interleaved slice acquisition times, (4) thresholding at 10% of the 98th percentile and maximum filtering of all voxels, (5) spatial smoothing with a 5 mm full width at half maximum Gaussian kernel using a 3D median filter and a brightness threshold of 0.75 * 50th percentile as implemented in SUSAN (Smith & Brady, 1997), (6) intensity normalization, (7) independent component analysis-based automatic removal of motion artifacts (ICA-AROMA) (Pruim et al., 2015), (8) nuisance regression to remove white matter and cerebrospinal fluids using the tissue probability masks distributed with the Data Processing Assistant for Resting-State fMRI (<http://rfmri.org/DPARSF>), (9) high-pass filtering with a 0.01 Hz cut-off to remove slow drifts, (10) registration of the high-resolution anatomical image to the MNI152 standard space template image (Montreal Neurological Institute) using a standard 12° of freedom search in FMRIB's Linear Image Registration Tool (FLIRT)

(Jenkinson et al., 2002; Jenkinson & Smith, 2001), refinement of the registration with a warp resolution of 10 mm in FMRIB's Nonlinear Image Registration Tool (FNIRT) (Andersson, Jenkinson, & Smith, 2007), and finally application of the resulting registration matrices to normalize the functional data. To verify that our results were not biased by global signal fluctuations, we repeated the analyses after including global signal regression (GSR) in the preprocessing (Supporting Information Materials S8 and S9).

2.5 | Identification of the ICNs

2.5.1 | ICA and dual-stage regression

To derive the ICNs from the preprocessed images of all subjects, we performed a group-level temporal concatenation independent component analysis (group-ICA) using FSL's Multivariate Exploratory Linear Optimized Decomposition into Independent Components (MELODIC) version 3.0 (Beckmann & Smith, 2004) with an estimation of 70 components (Abou Elseoud et al., 2011; Ray et al., 2013). An automatic estimation of the components yielded 263 independent components, which represented small voxel clusters rather than the large-scale ICNs that we were interested in. Next, inference on the estimated components was carried out using a mixture model and an alternative hypothesis testing approach with a threshold level of 0.5, which assumes an equal loss on false-positives and false-negatives (Beckmann, DeLuca, Devlin, & Smith, 2005). This resulted in spatial probability maps indicating, for each voxel, the probability that the voxel intensity exceeds the probability of being background noise. To classify the components into signal versus artifactual noise, we inspected the spatial probability maps visually using the criteria described in Kelly et al. (2010). This way, we classified 26 components as artifactual noise or cerebellar components (Supporting Information Materials S4). The remaining 44 components were classified as signal and entered into the template matching procedure described in the next section.

Next, we derived subject-specific versions of the spatial probability maps from the group-ICA and the associated time courses using a dual-stage regression (Beckmann, Mackay, Filippini, & Smith, 2009; Filippini et al., 2009). In stage one, the group-ICA spatial maps were regressed into each subject's series of functional images to give a set of time courses. In stage two, these time courses were normalized and then regressed into the same series of functional images to estimate a subject-specific set of spatial maps. Each spatial map reflects both the shape and the amplitude of the intrinsic connectivity within a component.

2.5.2 | Template matching procedure and computation of between-component interactions

To identify the components that best match the CEN, the SN, and the DMN, respectively, we applied a template matching procedure. Using spatial cross-correlations, we compared the 44 components classified as signal with spatial probability maps from an independent 20-dimension group-ICA reported in Smith et al. (2009) as well as with anatomical templates of the CEN, the SN and the DMN provided by Shirer et al. (2012, https://findlab.stanford.edu/functional_ROIs.html). We considered all components that showed a spatial correlation of

$r \geq .10$ with at least one of the templates. In cases of discrepancy between the two templates, visual inspection was used to find the best match.

Additionally, the spatial matching was compared with temporal interactions between the components. To this end, we computed a matrix of cross-correlations of the components' time courses for each subject using the FSLNets v0.5 package (<http://fsl.fmrib.ox.ac.uk/fsl/fslwiki/FSLNets>) run inside MATLAB R2015b (The MathWorks, Inc.). Specifically, we computed the z-transformed Pearson correlations of each pair of the subject-specific components' time courses to obtain between-component interactions. For each interaction, a one-sample t-test was computed that tested for deviations from zero at the group level. The matrix of z-transformed t-statistics of the between-component interactions is illustrated in Figure 3.

Integrating the results of the spatial and temporal cross-correlations, we matched components 19, 30, 31, 33, 40, 46, and 58 to the CEN, components 15, 24, and 54 to the SN, and components 5, 6, 18, 41, and 43 to the DMN (Figures 4, 5 and 6, Table 1). The remaining components clearly corresponded to visual, auditory or sensorimotor networks or did not directly match an ICN (Supporting Information Materials S5 and S6). It should be pointed out that component 19 shared spatial overlap with both the CEN and the SN, but that its peak clusters were located within the dlPFC (Table 1, Figure 4). Following the notion that the dlPFC is a major hub of the CEN (Menon, 2011; Seeley et al., 2007; Sridharan et al., 2008), we matched component 19 to the CEN. Component 24 showed spatial correlations with the SN as well as with the auditory network reported in Smith et al. (2009). Visual inspection, however, revealed that the peak clusters of component 24 were located in the anterior insula and the inferior frontal gyrus, which supported a matching with the SN (Table 1, Figure 5). Lastly, besides their overlaps with the DMN, components 41 and 43 also shared overlaps with the SN and CEN, respectively. The temporal cross-correlations, however, demonstrated stronger

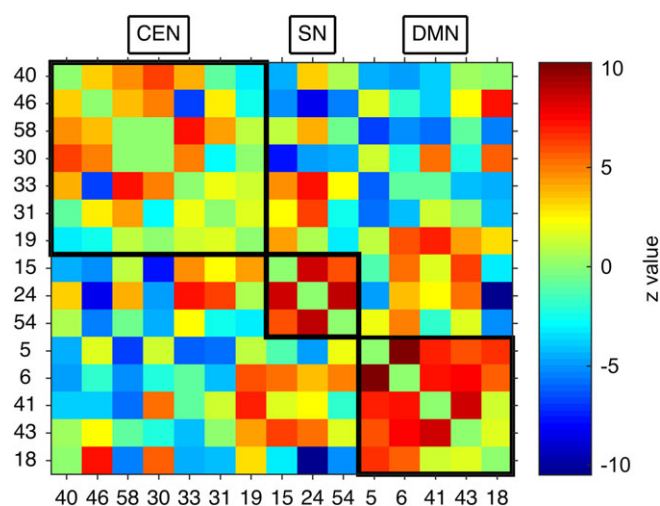


FIGURE 3 Temporal cross-correlations of the components matched to the CEN, the SN, and the DMN. Colors denote z-transformed t-statistics of pairwise Pearson correlations. CEN, central executive network; SN, salience network; DMN, default mode network [Color figure can be viewed at wileyonlinelibrary.com]

central executive network (CEN)

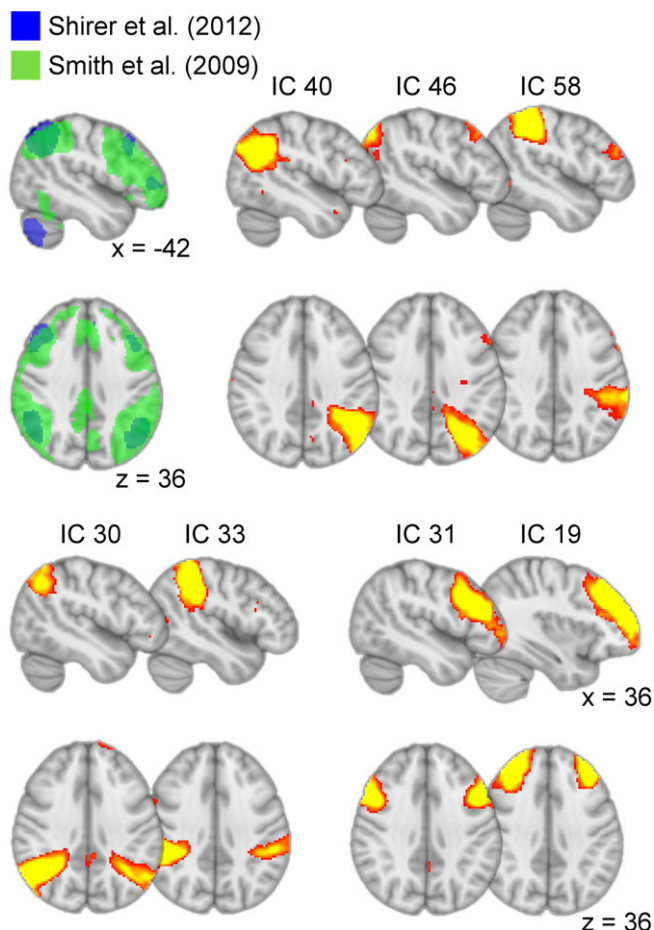


FIGURE 4 Central executive network (CEN). Left, the CEN as reported in Shirer et al. (2012) and the frontoparietal network as reported in Smith et al. (2009) in blue and green, respectively. Right, ICs from the ICA with 70 dimensions matching the CEN. Brain maps were thresholded from $Z = 3$ to $Z = 6$ (in a gradient from red to yellow), superimposed on the MNI152 standard space template image and displayed in radiological convention (left is right). IC, independent component [Color figure can be viewed at wileyonlinelibrary.com]

salience network (SN)

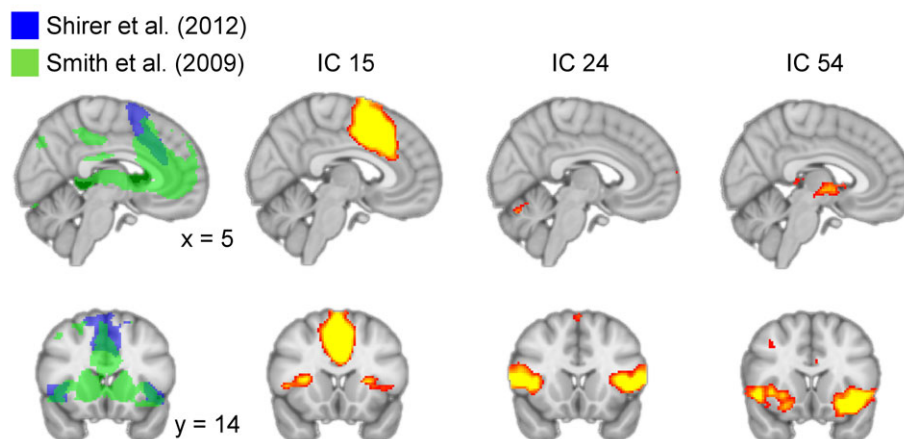


FIGURE 5 Salience network (SN). Left, the SN as reported in Shirer et al. (2012) and the executive control network as reported in Smith et al. (2009) in blue and green, respectively. Right, ICs from the ICA with 70 dimensions matching the SN. Brain maps were thresholded from $Z = 3$ to $Z = 6$ (in a gradient from red to yellow), superimposed on the MNI152 standard space template image and displayed in radiological convention (left is right). IC, independent component [Color figure can be viewed at wileyonlinelibrary.com]

similarities with the DMN components 5 and 6 (Figure 3), and therefore both components were matched with the DMN.

2.6 | Resting state fMRI data analysis

To test whether the intrinsic connectivity within the CEN, the SN or the DMN can explain individual differences in control-averse behavior, we applied general linear models using nonparametric permutation inference as implemented in the FSL function *randomise* (Winkler, Ridgway, Webster, Smith, & Nichols, 2014) within the respective ICA spatial map thresholded at $Z = 4$. For each general linear model we used the individual level of control-averse behavior as independent variable and the subject-specific spatial probability maps of the respective components as dependent variables. Each spatial map contains information on how well each voxel is integrated in the component. Statistical inference was based on nonparametric permutation tests using threshold-free cluster enhancement (TFCE) with 5,000 permutations (Nichols & Holmes, 2002; Smith & Nichols, 2009). To correct for multiple comparisons we applied family-wise error (FWE) correction. To visualize the results, we extracted the mean value across the largest significant cluster at $p_{FWE} < .05$ for each subject and plotted it against the individual level of control-averse behavior.

Finally, to test whether control-averse behavior was associated with between-component interactions, we analyzed the pairwise correlations of the components' time courses. More specifically, we used the individual level of control-averse behavior as dependent variable and the subject-wise z -transformed Pearson correlations between the subject-specific components' time courses as independent variables in robust regression analyses as implemented in the MATLAB R2015b Statistics and Machine Learning Toolbox function *robustfit*. To correct for multiple comparisons we applied Holm–Bonferroni correction. We visualized the results by plotting the z -transformed coefficients of the between-component correlations against the individual level of control-averse behavior.

TABLE 1 Results of the group-ICA and the spatial cross-correlations between the components and the templates of the CEN, SN, and DMN as provided by Smith et al. (2009) and Shirer et al. (2012)

IC	Cluster size	Max Z	Peak MNI coordinates			Peak location	Correlation with template	
			x	y	z		Smith et al. (2009)	Shirer et al. (2012)
Central executive network (CEN)								
40	3,331	11.40	−42	−50	36	IPL/supramarginal gyrus/angular gyrus	0.22	0.17
	106	4.79	50	−50	24	Superior temporal gyrus/IPL/ supramarginal gyrus/angular gyrus		
46	3,210	12.10	−30	−72	54	SPL	0.33	0.24
	124	5.14	20	−52	42	SPL		
58	3,715	12.10	−36	−40	50	IPL/postcentral gyrus	0.30	0.12
	145	6.42	−50	34	22	dIPFC/MFG		
	22	4.50	42	−36	56	IPL/postcentral gyrus		
30	3,450	13.90	46	−58	40	IPL/angular gyrus	0.32	0.23
	1,578	7.29	−34	−58	48	IPL/angular gyrus		
33	3,649	15.10	48	−40	42	IPL/supramarginal gyrus	0.31	0.16
	791	6.50	−52	−36	36	IPL		
	126	5.78	4	−40	64	Paracentral lobule		
31	3,431	12.50	50	24	26	dIPFC/MFG	0.20	0.13
	2,365	10.80	−44	12	34	dIPFC/MFG/precentral gyrus		
	30	4.72	−4	58	−12	OFC/medial frontal gyrus		
19	4,257	12.70	30	46	26	dIPFC/MFG	0.16	0.15
	2,228	10.20	−38	52	22	dIPFC/MFG		
Salience network (SN)								
15	4,211	20.00	0	16	46	ACC	0.22	0.48
	267	6.10	30	14	10	Insula		
	49	5.76	−26	16	8	Insula		
	31	4.94	36	48	32	SFG/MFG		
	23	4.73	−42	20	2	Insula		
24	2,476	10.40	52	22	6	Insula/IFG	0.04	0.10
	2,253	9.81	−46	22	6	Insula/IFG		
54	2,878	8.68	−16	4	−8	Putamen/insula/IFG/OFC	0.16	0.06
	2,580	8.58	18	2	−2	Putamen/insula/IFG/OFC		
	52	4.66	44	32	44	dIPFC/MFG		
	48	4.83	−2	−14	−8	Midbrain		
Default mode network (DMN)								
5	5,229	16.10	−6	58	−2	mPFC	0.25	0.45
	145	5.89	−2	−46	30	PCC		
6	7,776	17.80	−10	42	0	ACC	0.05	0.32
	23	5.18	−28	22	−4	OFC		
	22	6.84	14	20	−28	Insula		
41	4,310	13.10	6	52	28	dmPFC/SFG	0.07	0.26
43	3,817	14.20	−6	40	36	dmPFC/SFG	0.01	0.25
	29	5.69	−12	−2	16	Caudate		
18	4,626	15.80	−2	−60	40	PCC/precuneus	0.45	0.23
	45	4.78	8	58	−14	mPFC/medial frontal gyrus		

Results from the group-ICA are shown, thresholded at $Z \geq 4$ and cluster size >20 . IC = independent component; dIPFC = dorsolateral prefrontal cortex; MFG = middle frontal gyrus; SPL = superior parietal lobule; IPL = inferior parietal lobule; SFG = superior frontal gyrus; OFC = orbitofrontal cortex; dmPFC = dorsomedial prefrontal cortex; mPFC = medial prefrontal cortex; PCC = posterior cingulate cortex; ACC = anterior cingulate cortex; IFG = inferior frontal gyrus.

3 | RESULTS

3.1 | Behavior

First of all we assessed the subjects' individual levels of control-averse behavior by comparing their choices in two experimental conditions.

In the Free condition, subjects could choose freely among five levels of monetary allocations between themselves and another person, whereas in the Controlled condition, the other person requested a minimal monetary allocation of level two and thereby restricted the subjects' choices to more generous and fairer allocations. A

TABLE 2 Affects as assessed by trial-by-trial ratings in the Controlled compared with the Free condition

	Controlled condition		Free condition		Controlled > Free Wilcoxon signed rank test (two-tailed)		Hodges–Lehmann median of differences		
	M	SD	M	SD	Z stat	p	Estimator	95% confidence interval	
Unhappiness	1.99	0.67	1.50	0.51	4.95	<.001	−0.63	−0.88	−0.44
Anger	1.67	0.59	1.30	0.39	4.40	<.001	−0.50	−0.75	−0.31
Being controlled	2.17	0.90	1.64	0.80	4.39	<.001	−0.63	−0.94	−0.44

Sample size $N = 50$ subjects.

manipulation check confirmed that subjects indeed felt more controlled in the Controlled condition than in the Free condition as assessed by trial-by-trial affect ratings ($p < .001$, Table 2). Subjects also reported feeling unhappier and angrier in the Controlled than in the Free condition ($p < .001$, Table 2). At the aggregate level, subjects chose, on average, lower levels in the Controlled condition (mean $3.52 \pm SD 0.73$, median 3.44) than in the Free condition (mean $4.20 \pm SD 0.77$, median 4.44; Wilcoxon signed rank test, two-tailed, $Z = -4.83$, $p < .001$; Hodges–Lehmann median of differences = 0.88, 95% CI [0.66–1.13]; Figure 7). This statistical test was corrected for a bottom effect, following the procedure by Falk and Kosfeld (2006).

To verify that the behavior was not affected by the scanner environment, we compared the behavioral results with data from a behavioral study with $N = 42$ subjects (26 female; mean $22 \pm SD 4$ years) in a computer laboratory. The comparison confirmed that the behavior subjects displayed in the resting state fMRI study was remarkably similar to the behavior subjects showed in the behavioral study (see Supporting Information Materials S1–S3).

Next, we computed subjects' individual levels of control-averse behavior as the mean chosen level in the Free condition minus the mean chosen level in the Controlled condition. As illustrated by the histogram in Figure 7 the individual levels of control-averse behavior are well distributed. For completeness, the distributions of the chosen levels in each condition are depicted in the Supporting Information Materials S3. Male and female subjects did not differ in their

individual levels of control-averse behavior (Wilcoxon rank sum test, two-tailed, $Z = 1.21$, $p = .227$). Lastly, age was not significantly correlated with control-averse behavior (Spearman's $\rho = 0.01$, $p = .960$; $R^2 = 0.02$, $p = .382$).

3.2 | Functional connectivity within the SN predicts control-averse behavior

The first aim of the resting state fMRI analysis was to test whether the intrinsic dynamics within the CEN, the SN, and the DMN can predict individual differences in control-averse behavior. First of all we identified the components that best matched the CEN, the SN, and the DMN using a template matching procedure (Figures 3, 4, 5 and 6, Table 1). We then computed, for each subject and each component, spatial probability maps that indicate the voxel-wise amplitude of the intrinsic connectivity within the respective component. These spatial probability maps were then entered into regression analyses with nonparametric permutation inference using TFCE.

The regression analyses revealed that the functional connectivity within the SN component 15, specifically in the dorsal ACC, correlates positively with the individual level of control-averse behavior (peak MNI coordinates $[-2, 26, 46]$, cluster size = 2,994 voxels, peak $p_{FWE} < .001$, FWE-corrected for multiple comparisons across space using TFCE; Figure 8). The results remained robust after exclusion of three outliers with a functional connectivity greater than 2 SD from the

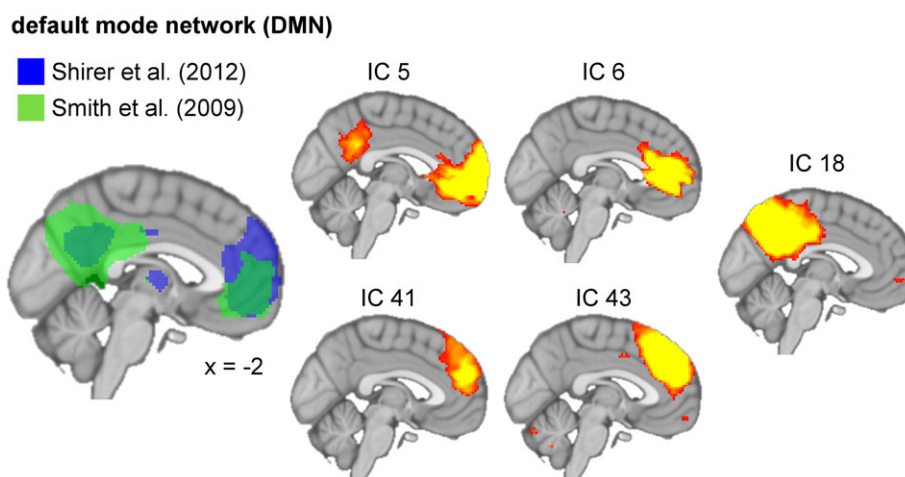


FIGURE 6 Default mode network (DMN). Left, the DMN as reported in Shirer et al. (2012) and Smith et al. (2009) in blue and green, respectively. Right, ICs from the ICA with 70 dimensions matching the DMN. Brain maps were thresholded from $Z = 3$ to $Z = 6$ (in a gradient from red to yellow), superimposed on the MNI152 standard space template image and displayed in radiological convention (left is right). IC, independent component [Color figure can be viewed at wileyonlinelibrary.com]

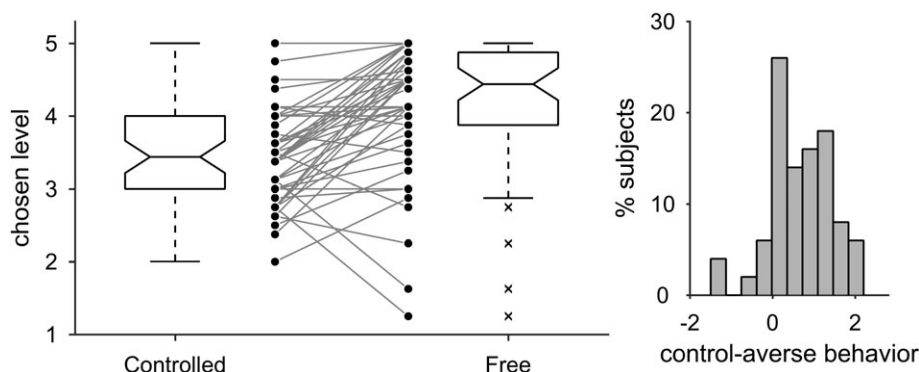


FIGURE 7 Control-averse behavior. Boxplots show the chosen levels in the Controlled and the Free condition. The central mark of each box shows the median, the box edges show the 25th and 75th percentiles, the whiskers represent the limit beyond which data points are considered outliers (shown as crosses), and the connected data points show individual subjects' means. The histogram shows the distribution of subjects' individual levels of control-averse behavior, computed as the mean chosen level in the Free condition minus the mean chosen level in the Controlled condition. Data from $N = 50$ subjects are shown

mean (Supporting Information Materials S7). No other component showed significant correlations, even at a more liberal threshold of $p_{FWE} < .10$. The results were highly similar when using GSR during preprocessing (see Supporting Information Materials S8 and S9).

3.3 | Association of control-averse behavior and between-component interactions

Finally, we examined the association of control-averse behavior and between-component interactions. To do this, we ran robust regression analyses using the individual level of control-averse behavior as dependent variable and the subject-wise z -transformed coefficients of the between-component correlations as independent variables. Due to the specific association between the SN component 15 and

control-averse behavior and the SN's proposed key role in switching between activations and deactivations of the CEN and the DMN (Menon, 2011; Menon & Uddin, 2010), we focused on interactions of the SN component 15 with components of the CEN and the DMN.

After Holm-Bonferroni correction, no interaction was significantly correlated with control-averse behavior. At an uncorrected statistical threshold, interactions between the SN component 15 and component 58, representing a left fronto-parietal component of the CEN, showed a negative association with control-averse behavior ($\beta = -1.36$, $R^2 = .10$, $p_{\text{uncorrected}} = .026$; Figure 9). Although the low R^2 coefficient of determination warrants caution, this result could motivate further investigations into whether a more negative temporal coupling between the SN and the CEN is associated with greater individual levels of control-averse behavior.

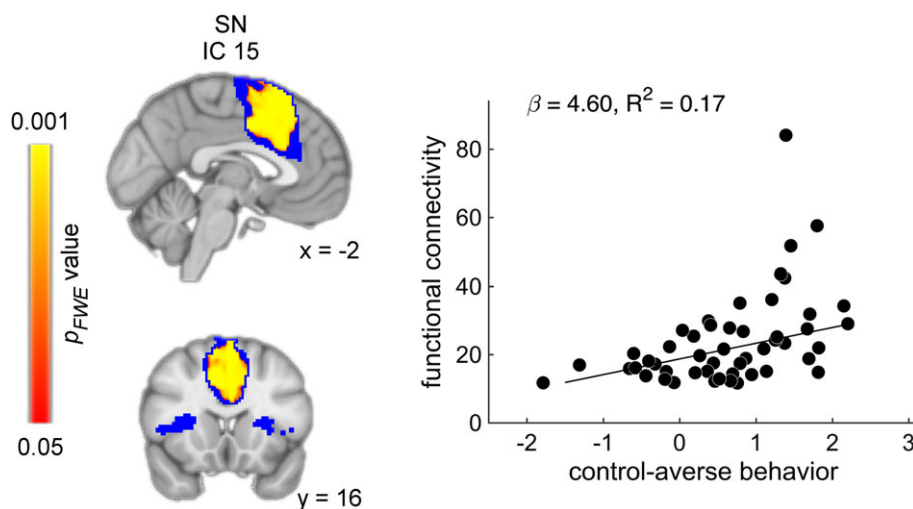


FIGURE 8 Control-averse behavior correlates positively with functional connectivity within the SN. Left, voxels showing significant associations ($.001 < p_{FWE} < .05$) in a gradient from yellow to red overlaid on top of the SN component 15 (in blue) as defined by the ICA spatial map thresholded at $Z = 4$, superimposed on the MNI152 standard space template image. Right, scatterplot showing the individual level of control-averse behavior plotted against the mean functional connectivity across the largest significant cluster in the dorsal ACC. The regression line was estimated using robust regression. Observations are jittered along the x-axis to reduce overlap for visualization. The results remained robust after exclusion of outliers (Supporting Information Materials S7). SN, salience network; ACC, anterior cingulate cortex; IC, independent component [Color figure can be viewed at wileyonlinelibrary.com]

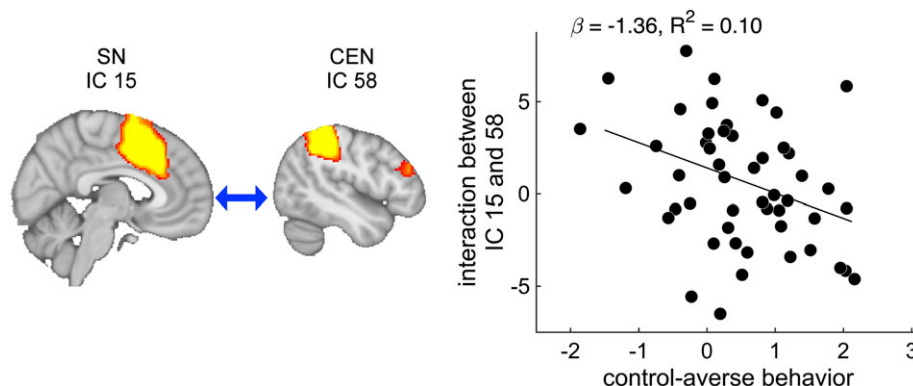


FIGURE 9 Interactions between the SN and the CEN correlate negatively with control-averse behavior. Left, spatial probability maps of the components. Right, the graph shows the z-transformed coefficient of the subject-wise correlations between the indicated components, plotted against the individual level of control-averse behavior. The regression line was estimated using robust regression. Observations are jittered along the x-axis to reduce overlap for visualization. SN, salience network; CEN, central executive network; IC, independent component [Color figure can be viewed at wileyonlinelibrary.com]

4 | DISCUSSION

This study investigated whether individual differences in control-averse behavior could be explained by stable characteristics of three core intrinsic brain networks at rest, the CEN, the SN and the DMN. We found that the functional connectivity within the SN positively predicted individual control-averse behavior. Specifically, subjects with a more prominent connectivity hub in the dorsal ACC showed greater levels of control-averse behavior. Interestingly, this result was specific to the SN and was not found in the CEN or DMN.

Control-averse behavior is a ubiquitous phenomenon that affects social interactions in many domains of our society. When people sense that their freedom of choice is restricted, some people will comply, but others will act against the restriction. The fact that people differ in their degree of control-averse behavior has been described in previous studies. Yet, the neurobiological basis of individual differences in control-averse behavior has not been fully elucidated. To illuminate this issue, we assessed control-averse behavior in a decision making task with real (monetary) consequences. This feature helps to overcome limitations that would be associated with self-reports, such as the need for introspection or the proneness to cognitive biases and social desirability effects, and it therefore ensures a higher ecological validity. Moreover, it could be argued that actual decisions are more informative of subjects' preferences than subjects' reflections on their past behavior or their imagination of hypothetical scenarios. Using this ecologically valid measurement of control-averse behavior, we were able to identify a possible source of the heterogeneity in control-averse behavior in the intrinsic neural dynamics of the SN.

The SN has been associated with the stable maintenance of cognitive task sets and thereby the display of stable preferences over an entire task (Dosenbach et al., 2006, 2007). In line with this argument, our data suggest that the intrinsic connectivity within the SN reflects a brain characteristic that determines the individual preference for control-averse behavior. Moreover, the SN is a key network in the detection of and attention reorientation to salient external and internal stimuli (Menon, 2011; Seeley et al., 2007). Further, the SN, but not the CEN or DMN, has been shown to uniquely decode individual

behavioral tendencies for cooperation (Hahn et al., 2015), a central human social behavior that requires attending to own- and other-related benefits. Complementing this research, we find that connectivity within the SN, as opposed to the CEN or DMN, is associated with individual control-averse behavior in a task that involves attending to and weighing the own and another person's profit. Considering its key role in responses to salient stimuli, a stronger connectivity of the dorsal ACC within the SN could imply an increased individual propensity to assign saliency to the exogenous control of one's choices and thus to react to the control.

Corroborating the role of the ACC and the insula in salience processing, both regions are also considered central nodes in a neural network that is anchored around the amygdala and responds to aversive stimuli. This aversion network has been shown to mediate both the passive perception of as well as the more complex cognitive or behavioral responses to aversive stimuli (Bickart, Hollenbeck, Barrett, & Dickerson, 2012; Hayes & Northoff, 2011). Activation in the dorsal ACC, in particular, has been shown to increase during social distress (Eisenberger, Lieberman, & Williams, 2003), supporting the involvement of the dorsal ACC in responses to aversive social events. Our findings extend this research by linking the individual response to the aversive social event of being controlled by another person to the intrinsic connectivity centered on the dorsal ACC.

Furthermore, the SN has been shown to play a critical role in switching between the engagement of the CEN and the DMN in resting state fMRI and cognitive tasks (Bressler & Menon, 2010; Goulden et al., 2014; Menon & Uddin, 2010; Sridharan et al., 2008). Whereas an engagement of the CEN might facilitate goal-directed behavior (Menon, 2011; Seeley et al., 2007), an engagement of the DMN might facilitate self-related and social thoughts (Li et al., 2014; Mars et al., 2012; Menon, 2011). Although the neural capacity to balance goal-directed behavior and social thoughts seems relevant to control-averse behavior, we did not find a correlation between the SN and the CEN or DMN that significantly corresponded to the individual level of control-averse behavior. At an uncorrected statistical threshold, however, we found a negative association between control-averse behavior and the intrinsic connectivity between the SN and

the CEN. Albeit nonsignificant, this association is in line with a recent finding that a decreased intrinsic connectivity between the SN and the CEN is associated with less generous choices in a trust game (Cáceda et al., 2015). The finding also links the resting state fMRI data to the task-related fMRI data, which revealed an association between the individual level of control-averse behavior and an increased functional connectivity between two core regions of the CEN, the inferior parietal lobule and the dlPFC, in the Controlled as opposed to the Free condition (Rudorf et al., 2018). Similar to the resting state fMRI data, the intrinsic connectivity between these two CEN nodes, that is, the residual functional connectivity after controlling for the events of the task, did not predict control-averse behavior. Although ICNs at rest have been shown to correspond well with ICNs during tasks (Smith et al., 2009), they also display lower global efficiency and higher modularity compared with task-related coactivation networks (Di, Gohel, Kim, & Biswal, 2013; Kitzbichler, Henson, Smith, Nathan, & Bullmore, 2011), suggesting an energy-saving reduction of global information transmission and between network integrations during rest (Bullmore & Sporns, 2012). To further investigate this issue, future studies could test specifically whether changes in between-network integrations of the SN and CEN during rest compared with task demands might contribute to the individual differences in control-averse behavior, for example, by using effective connectivity or graph theoretical analyses.

By assessing the intrinsic neural connectivity at rest, the current study has identified a neural trait underlying control-averse behavior, that is, an objective, task-independent neural measurement that is stable across time and capable of differentiating between individuals, similar to a neural fingerprint (Finn et al., 2015; Nash et al., 2015). The evidence for a neural trait underlying control-averse behavior complements previous work that has described individual differences in control aversion at the behavioral level (Falk & Kosfeld, 2006; Schmelz & Ziegelmeyer, 2015; Ziegelmeyer et al., 2012). A more thorough understanding of the association between neural traits and control-averse behavior not only adds to a more comprehensive model of control aversion, but could also be applied to the clinical context. For example, if assessing patients' neural traits could help identifying candidates for control-averse behavior, treatment plans could be adapted accordingly to increase the patients' compliance to the treatment and thereby the treatment's overall efficiency. One great advantage of resting state fMRI is that a short resting state scan is much more feasible in the daily clinical routine than a more complex task-based fMRI procedure (Finn et al., 2015).

5 | CONCLUSION

Using a data-driven ICA approach, this study has identified a new link between the intrinsic functional brain organization and a ubiquitous social phenomenon, control-averse behavior. In particular, our findings suggest that the heterogeneity in control-averse behavior might originate in distinct patterns of connectivity centered on the salience network (SN). These findings therefore provide the first evidence of a neural trait of control-averse behavior.

ACKNOWLEDGMENTS

This project was supported by a grant to DK by the Mens Sana Foundation. Calculations were performed on the University of Bern Linux high performance computing cluster (UBELIX, <http://www.id.unibe.ch/hpc>).

ORCID

Sarah Rudorf  <http://orcid.org/0000-0002-3274-945X>

REFERENCES

- Abou Elseoud, A., Littow, H., Remes, J., Starck, T., Nikkinen, J., Nissilä, J., ... Kiviniemi, V. (2011). Group-ICA model order highlights patterns of functional brain connectivity. *Frontiers in Systems Neuroscience*, 5(37), 1–18. <http://doi.org/10.3389/fnsys.2011.00037>
- Andersson, J. L. R., Jenkinson, M., & Smith, S. (2007). Non-linear registration aka Spatial normalisation. FMRIB Technical Report TR07JA2.
- Andrews-Hanna, J. R., Reidler, J. S., Sepulcre, J., Poulin, R., & Buckner, R. L. (2010). Functional-anatomic fractionation of the brain's default network. *Neuron*, 65(4), 550–562. <http://doi.org/10.1016/j.neuron.2010.02.005>
- Beckmann, C. F., DeLuca, M., Devlin, J. T., & Smith, S. M. (2005). Investigations into resting-state connectivity using independent component analysis. *Philosophical Transactions: Biological Sciences*, 360(1457), 1001–1013. <http://doi.org/https://doi.org/10.1098/rstb.2005.1634>
- Beckmann, C. F., Mackay, C. E., Filippini, N., & Smith, S. M. (2009). Group comparison of resting-state FMRI data using multi-subject ICA and dual regression. *Organization for Human Brain Mapping Annual Meeting. Neuroimage*, 47, 148. [http://doi.org/10.1016/S1053-8119\(09\)71511-3](http://doi.org/10.1016/S1053-8119(09)71511-3)
- Beckmann, C. F., & Smith, S. M. (2004). Probabilistic independent component analysis for functional magnetic resonance imaging. *IEEE Transactions on Medical Imaging*, 23(2), 137–152. <http://doi.org/10.1109/TMI.2003.822821>
- Betsch, C., & Böhm, R. (2016). Detrimental effects of introducing partial compulsory vaccination: Experimental evidence. *European Journal of Public Health*, 26(3), 378–381. <http://doi.org/10.1093/eurpub/ckv154>
- Bickart, K. C., Hollenbeck, M. C., Barrett, L. F., & Dickerson, B. C. (2012). Intrinsic amygdala-cortical functional connectivity predicts social network size in humans. *Journal of Neuroscience*, 32(42), 14729–14741. <http://doi.org/10.1523/JNEUROSCI.1599-12.2012>
- Biswal, B. B., Mennes, M., Zuo, X.-N., Gohel, S., Kelly, C., Smith, S. M., ... Milham, M. P. (2010). Toward discovery science of human brain function. *Proceedings of the National Academy of Sciences*, 107(10), 4734–4739. <http://doi.org/10.1073/pnas.0911855107>
- Biswal, B., Yetkin, F., Haughton, V., & Hyde, J. (1995). Functional connectivity in the motor cortex of resting human brain using Echo-planar MRI. *Magnetic Resonance in Medicine*, 34(9), 537–541. <http://doi.org/10.1002/mrm.1910340409>
- Bradley, M., & Lang, P. J. (1994). Measuring emotion: The self-assessment manikin and the semantic differential. *Journal of Behavior Therapy and Experimental Psychiatry*, 25(1), 49–59. [http://doi.org/https://doi.org/10.1016/0005-7916\(94\)90063-9](http://doi.org/https://doi.org/10.1016/0005-7916(94)90063-9)
- Bressler, S. L., & Menon, V. (2010). Large-scale brain networks in cognition: Emerging methods and principles. *Trends in Cognitive Sciences*, 14(6), 277–290. <http://doi.org/10.1016/j.tics.2010.04.004>
- Bullmore, E., & Sporns, O. (2012). The economy of brain network organization. *Nature Reviews Neuroscience*, 13(5), 336–349. <http://doi.org/10.1038/nrn3214>
- Cáceda, R., James, G. A., Gutman, D. A., & Kilts, C. D. (2015). Organization of intrinsic functional brain connectivity predicts decisions to reciprocate social behavior. *Behavioural Brain Research*, 292, 478–483. <http://doi.org/10.1016/j.bbr.2015.07.008>
- Chen, A. C., Oathes, D. J., Chang, C., Bradley, T., Zhou, Z.-W., Williams, L. M., ... Etkin, A. (2013). Causal interactions between fronto-parietal central executive and default-mode networks in humans. *Proceedings of the National Academy of Sciences*, 110(49), 19944–19949. <http://doi.org/10.1073/pnas.1311772110>

- Damoiseaux, J. S., Rombouts, S. A. R. B., Barkhof, F., Scheltens, P., Stam, C. J., Smith, S. M., & Beckmann, C. F. (2006). Consistent resting-state networks across healthy subjects. *Proceedings of the National Academy of Sciences*, 103(37), 13848–13853. <http://doi.org/10.1073/pnas.0601417103>
- De las Cuevas, C., Peñate, W., Betancort, M., & de Rivera, L. (2014). Psychological reactance in psychiatric patients: Examining the dimensionality and correlates of the Hong psychological reactance scale in a large clinical sample. *Personality and Individual Differences*, 70, 85–91. <http://doi.org/10.1016/j.paid.2014.06.027>
- Di, X., Gohel, S., Kim, E. H., & Biswal, B. B. (2013). Task vs. rest—Different network configurations between the coactivation and the resting-state brain networks. *Frontiers in Human Neuroscience*, 7, 1–9. <http://doi.org/10.3389/fnhum.2013.00493>
- Dillard, J. P., & Shen, L. (2005). On the nature of reactance and its role in persuasive health communication. *Communication Monographs*, 72(2), 144–168. <http://doi.org/10.1080/03637750500111815>
- Dosenbach, N. U. F., Fair, D. A., Miezin, F. M., Cohen, A. L., Wenger, K. K., Dosenbach, R. A. T., ... Petersen, S. E. (2007). Distinct brain networks for adaptive and stable task control in humans. *Proceedings of the National Academy of Sciences*, 104(26), 11073–11078. <http://doi.org/10.1073/pnas.0704320104>
- Dosenbach, N. U. F., Visscher, K. M., Palmer, E. D., Miezin, F. M., Wenger, K. K., Kang, H. C., ... Petersen, S. E. (2006). A Core system for the implementation of task sets. *Neuron*, 50(5), 799–812. <http://doi.org/10.1016/j.neuron.2006.04.031>
- Eisenberger, N. I., Lieberman, M. D., & Williams, K. D. (2003). Does rejection hurt? An fMRI study of social exclusion. *Science*, 302, 290–292. <http://doi.org/10.1126/science.1089134>
- Elton, A., & Gao, W. (2014). Divergent task-dependent functional connectivity of executive control and salience networks. *Cortex*, 51(1), 56–66. <http://doi.org/10.1016/j.cortex.2013.10.012>
- Falk, A., & Kosfeld, M. (2006). The hidden costs of control. *The American Economic Review*, 96(5), 1611–1630. <http://doi.org/10.1257/aer.96.5.1611>
- Finn, E. S., Shen, X., Scheinost, D., Rosenberg, M. D., Huang, J., Chun, M. M., ... Constable, R. T. (2015). Functional connectome fingerprinting: Identifying individuals using patterns of brain connectivity. *Nature Neuroscience*, 18(11), 1664–1671. <http://doi.org/10.1038/nn.4135>
- Filippini, N., MacIntosh, B. J., Hough, M. G., Goodwin, G. M., Frisoni, G. B., Smith, S. M., Matthews, P. M., Beckmann, C. F., Mackay, C. E. (2009). Distinct patterns of brain activity in young carriers of the APOE-epsilon4 allele. *Proc Natl Acad Sci USA*, 106(11), 7209–7214. <http://doi.org/10.1073/pnas.0811879106>
- Fox, M. D., Snyder, A. Z., Vincent, J. L., & Raichle, M. E. (2007). Intrinsic fluctuations within cortical systems account for intertrial variability in human behavior. *Neuron*, 56(1), 171–184. <http://doi.org/10.1016/j.neuron.2007.08.023>
- Gordon, E. M., Stollstorff, M., & Vaidya, C. J. (2012). Using spatial multiple regression to identify intrinsic connectivity networks involved in working memory performance. *Human Brain Mapping*, 33(7), 1536–1552. <http://doi.org/10.1002/hbm.21306>
- Goulden, N., Khusnulina, A., Davis, N. J., Bracewell, R. M., Bokde, A. L., McNulty, J. P., & Mullins, P. G. (2014). The salience network is responsible for switching between the default mode network and the central executive network: Replication from DCM. *NeuroImage*, 99, 180–190. <http://doi.org/10.1016/j.neuroimage.2014.05.052>
- Greicius, M. D., Krasnow, B., Reiss, A. L., & Menon, V. (2003). Functional connectivity in the resting brain: A network analysis of the default mode hypothesis. *Proceedings of the National Academy of Sciences*, 100(1), 253–258. <http://doi.org/10.1073/pnas.0135058100>
- Hahn, T., Notebaert, K., Anderl, C., Reicherts, P., Wieser, M., Kopf, J., ... Windmann, S. (2015). Reliance on functional resting-state network for stable task control predicts behavioral tendency for cooperation. *NeuroImage*, 118, 231–236. <http://doi.org/10.1016/j.neuroimage.2015.05.093>
- Hayes, D. J., & Northoff, G. (2011). Identifying a network of brain regions involved in aversion-related processing: A cross-species translational investigation. *Frontiers in Integrative Neuroscience*, 5(49), 1–21. <http://doi.org/10.3389/fnint.2011.00049>
- Hornik, R., Jacobsohn, L., Orwin, R., Piesse, A., & Kalton, G. (2008). Effects of the national youth anti-drug media campaign on youths. *American Journal of Public Health*, 98(12), 2229–2236. <http://doi.org/10.2105/AJPH.2007.125849>
- Jenkinson, M., Bannister, P., Brady, M., & Smith, S. (2002). Improved optimization for the robust and accurate linear registration and motion correction of brain images. *NeuroImage*, 17(2), 825–841. [http://doi.org/10.1016/S1053-8119\(02\)91132-8](http://doi.org/10.1016/S1053-8119(02)91132-8)
- Jenkinson, M., Beckmann, C. F., Behrens, T. E. J., Woolrich, M. W., & Smith, S. M. (2012). FSL. *NeuroImage*, 62(2), 782–790. <http://doi.org/10.1016/j.neuroimage.2011.09.015> FSL.
- Jenkinson, M., & Smith, S. (2001). A global optimisation method for robust affine registration of brain images. *Medical Image Analysis*, 5(2), 143–156. [http://doi.org/10.1016/S1361-8415\(01\)00036-6](http://doi.org/10.1016/S1361-8415(01)00036-6)
- Kelly, R. E., Alexopoulos, G. S., Wang, Z., Gunning, F. M., Murphy, C. F., Morimoto, S. S., ... Hoptman, M. J. (2010). Visual inspection of independent components: Defining a procedure for artifact removal from fMRI data. *Journal of Neuroscience Methods*, 189(2), 233–245. <http://doi.org/10.1016/j.jneumeth.2010.03.028>
- Kelly, A. M. C., Uddin, L. Q., Biswal, B. B., Castellanos, F. X., & Milham, M. P. (2008). Competition between functional brain networks mediates behavioral variability. *NeuroImage*, 39(1), 527–537. <http://doi.org/10.1016/j.neuroimage.2007.08.008>
- Kitzbichler, M. G., Henson, R. N. A., Smith, M. L., Nathan, P. J., & Bullmore, E. T. (2011). Cognitive effort drives workspace configuration of human brain functional networks. *Journal of Neuroscience*, 31(22), 8259–8270. <http://doi.org/10.1523/JNEUROSCI.0440-11.2011>
- Laird, A. R., Riedel, M. C., Okoe, M., Jianu, R., Ray, K. L., Eickhoff, S. B., ... Sutherland, M. T. (2017). Heterogeneous fractionation profiles of meta-analytic coactivation networks. *NeuroImage*, 149(February), 424–435. <http://doi.org/10.1016/j.neuroimage.2016.12.037>
- Li, W., Mai, X., & Liu, C. (2014). The default mode network and social understanding of others: What do brain connectivity studies tell us. *Frontiers in Human Neuroscience*, 8(74), 1–15. <http://doi.org/10.3389/fnhum.2014.00074>
- Markett, S., Montag, C., & Reuter, M. (2018). Network neuroscience and personality. *Personality Neuroscience*, 1–14. <http://doi.org/10.1017/pen.2018.12>
- Mars, R. B., Neubert, F., Maryann, P., Sallet, J., Toni, I., & Rushworth, M. F. S. (2012). On the relationship between the “default mode network” and the “social brain.”. *Frontiers in Human Neuroscience*, 6(189), 1–9. <http://doi.org/10.3389/fnhum.2012.00189>
- Mendoza, J. P., Wielhouwer, J. L., & Kirchler, E. (2017). The backfiring effect of auditing on tax compliance. *Journal of Economic Psychology*, 62, 284–294. <http://doi.org/10.1016/j.joep.2017.07.007>
- Mennes, M., Zuo, X. N., Kelly, C., Di Martino, A., Zang, Y. F., Biswal, B., ... Milham, M. P. (2011). Linking inter-individual differences in neural activation and behavior to intrinsic brain dynamics. *NeuroImage*, 54(4), 2950–2959. <http://doi.org/10.1016/j.neuroimage.2010.10.046>
- Menon, V. (2011). Large-scale brain networks and psychopathology: A unifying triple network model. *Trends in Cognitive Sciences*, 15(10), 483–506. <http://doi.org/10.1016/j.tics.2011.08.003>
- Menon, V., & Uddin, L. Q. (2010). Saliency, switching, attention and control: A network model of insula function. *Brain Structure and Function*, 214(5–6), 655–667. <http://doi.org/10.1007/s00429-010-0262-0>
- Miron, A. M., & Brehm, J. W. (2006). Reactance Theory-40 years later. *Zeitschrift für Sozialpsychologie*, 37(1), 9–18. <http://doi.org/10.1024/0044-3514.37.1.3>
- Murphy, K. (2005). Regulating more effectively: The relationship between procedural justice, legitimacy, and tax non-compliance. *Journal of Law and Society*, 32(4), 562–589.
- Nash, K., Gianotti, L. R. R., & Knoch, D. (2015). A neural trait approach to exploring individual differences in social preferences. *Frontiers in Behavioral Neuroscience*, 8(258), 1–8. <http://doi.org/10.3389/fnbeh.2014.00458>
- Nichols, T. E., & Holmes, A. P. (2002). Nonparametric permutation tests for functional neuroimaging: A primer with examples. *Human Brain Mapping*, 15(1), 1–25. <http://doi.org/10.1002/hbm.1058>
- Pruim, R. H. R., Mennes, M., van Rooij, D., Llera, A., Buitelaar, J. K., & Beckmann, C. F. (2015). ICA-AROMA: A robust ICA-based strategy for

- removing motion artifacts from fMRI data. *NeuroImage*, 112, 267–277. <http://doi.org/10.1016/j.neuroimage.2015.02.064>
- Raichle, M. E., MacLeod, A. M., Snyder, A. Z., Powers, W. J., Gusnard, D. A., & Shulman, G. L. (2001). A default mode of brain function. *Proceedings of the National Academy of Sciences of the United States of America*, 98(2), 676–682. <http://doi.org/10.1073/pnas.98.2.676>
- Ray, K. L., McKay, D. R., Fox, P. M., Riedel, M. C., Uecker, A. M., Beckmann, C. F., ... Laird, A. R. (2013). ICA model order selection of task co-activation networks. *Frontiers in Neuroscience*, 7(237), 1–12. <http://doi.org/10.3389/fnins.2013.00237>
- Rudolf, S., Schmelz, K., Baumgartner, T., Wiest, R., Fischbacher, U., & Knoch, D. (2018). Neural mechanisms underlying individual differences in control-averse behavior. *The Journal of Neuroscience*, 38(22), 5196–5208. <http://doi.org/10.1523/JNEUROSCI.0047-18.2018>
- Schmelz, K., & Ziegelmeyer, A. (2015). Social distance and control aversion: Evidence from the internet and the laboratory. *Thurgau Institute of Economics Research Paper Series*, 100, 1–25.
- Seeley, W. W., Menon, V., Schatzberg, A. F., Keller, J., Glover, G. H., Kenna, H., ... Greicius, M. D. (2007). Dissociable intrinsic connectivity networks for salience processing and executive control. *The Journal of Neuroscience*, 27(9), 2349–2356. <http://doi.org/10.1523/JNEUROSCI.5587-06.2007>
- Shehzad, Z., Kelly, A. M. C., Reiss, P. T., Gee, D. G., Gotimer, K., Uddin, L. Q., ... Milham, M. P. (2009). The resting brain: Unconstrained yet reliable. *Cerebral Cortex*, 19(10), 2209–2229. <http://doi.org/10.1093/cercor/bhn256>
- Shirer, W. R., Ryali, S., Rykhlevskaia, E., Menon, V., & Greicius, M. D. (2012). Decoding subject-driven cognitive states with whole-brain connectivity patterns. *Cerebral Cortex*, 22, 158–165. <http://doi.org/10.1093/cercor/bhr099>
- Smith, S. M. (2002). Fast robust automated brain extraction. *Human Brain Mapping*, 17(3), 143–155. <http://doi.org/10.1002/hbm.10062>
- Smith, S. M., & Brady, J. M. (1997). SUSAN—A new approach to low level image processing. *International Journal of Computer Vision*, 23(1), 45–78. <http://doi.org/10.1023/A:1007963824710>
- Smith, S. M., Fox, P. M. T., Miller, K. L., Glahn, D. C., Fox, P. M. T., Mackay, C. E., ... Beckmann, C. F. (2009). Correspondence of the brain's functional architecture during activation and rest. *Proceedings of the National Academy of Sciences*, 106(31), 13040–13045. <http://doi.org/10.1073/pnas.0905267106>
- Smith, S. M., & Nichols, T. E. (2009). Threshold-free cluster enhancement: Addressing problems of smoothing, threshold dependence and localisation in cluster inference. *NeuroImage*, 44(1), 83–98. <http://doi.org/10.1016/j.neuroimage.2008.03.061>
- Sridharan, D., Levitin, D. J., & Menon, V. (2008). A critical role for the right fronto-insular cortex in switching between central-executive and default-mode networks. *Proceedings of the National Academy of Sciences*, 105(34), 12569–12574. <http://doi.org/10.1073/pnas.0800005105>
- Tavor, I., Jones, O. P., Mars, R. B., Smith, S. M., Behrens, T. E., & Jbabdi, S. (2016). Task-free MRI predicts individual differences in brain activity during task performance. *Science*, 352(6282), 216–220. <http://doi.org/https://doi.org/10.1126/science.aad8127>
- Van den Heuvel, M. P., & Hulshoff Pol, H. E. (2010). Exploring the brain network: A review on resting-state fMRI functional connectivity. *European Neuropsychopharmacology*, 20(8), 519–534. <http://doi.org/10.1016/j.euroneuro.2010.03.008>
- White, T. P., Joseph, V., Francis, S. T., & Liddle, P. F. (2010). Aberrant salience network (bilateral insula and anterior cingulate cortex) connectivity during information processing in schizophrenia. *Schizophrenia Research*, 123, 105–115. <http://doi.org/10.1016/j.schres.2010.07.020>
- Wiiium, N., Aarø, L. E., & Hetland, J. (2009). Psychological reactance and adolescents' attitudes toward tobacco-control measures. *Journal of Applied Social Psychology*, 39(7), 1718–1738. <http://doi.org/10.1111/j.1559-1816.2009.00501.x>
- Winkler, A. M., Ridgway, G. R., Webster, M. A., Smith, S. M., & Nichols, T. E. (2014). Permutation inference for the general linear model. *NeuroImage*, 92, 381–397. <http://doi.org/10.1016/j.neuroimage.2014.01.060>
- Xiong, J., Parsons, L. M., Gao, J.-H., & Fox, P. T. (1999). Interregional connectivity to primary motor cortex revealed using MRI resting state images. *Human Brain Mapping*, 8(2–3), 151–156. [http://doi.org/10.1002/\(sici\)1097-0193\(1999\)8:2/3<151::aid-hbm13>3.0.co;2-5](http://doi.org/10.1002/(sici)1097-0193(1999)8:2/3<151::aid-hbm13>3.0.co;2-5)
- Yu, E., Liao, Z., Tan, Y., Qiu, Y., Zhu, J., Han, Z., ... Ding, Z. (2017). High-sensitivity neuroimaging biomarkers for the identification of amnesic mild cognitive impairment based on resting-state fMRI and a triple network model. *Brain Imaging and Behavior*, 1–14. <http://doi.org/10.1007/s11682-017-9727-6>
- Ziegelmeyer, A., Schmelz, K., & Ploner, M. (2012). Hidden costs of control: Four repetitions and an extension. *Experimental Economics*, 15(2), 323–340. <http://doi.org/10.1007/s10683-011-9302-8>
- Zuo, X. N., Kelly, C., Adelstein, J. S., Klein, D. F., Castellanos, F. X., & Milham, M. P. (2010). Reliable intrinsic connectivity networks: Test-retest evaluation using ICA and dual regression approach. *NeuroImage*, 49(3), 2163–2177. <http://doi.org/10.1016/j.neuroimage.2009.10.080>

SUPPORTING INFORMATION

Additional supporting information may be found online in the Supporting Information section at the end of the article.

How to cite this article: Rudolf S, Baumgartner T, Markett S, et al. Intrinsic connectivity networks underlying individual differences in control-averse behavior. *Hum Brain Mapp*. 2018; 1–13. <https://doi.org/10.1002/hbm.24328>